RESEARCH ARTICLE | JUNE 22 2023

A multiscale approach to coupled nuclear and electronic dynamics. II. Exact and approximated evaluation of nonradiative transition rates

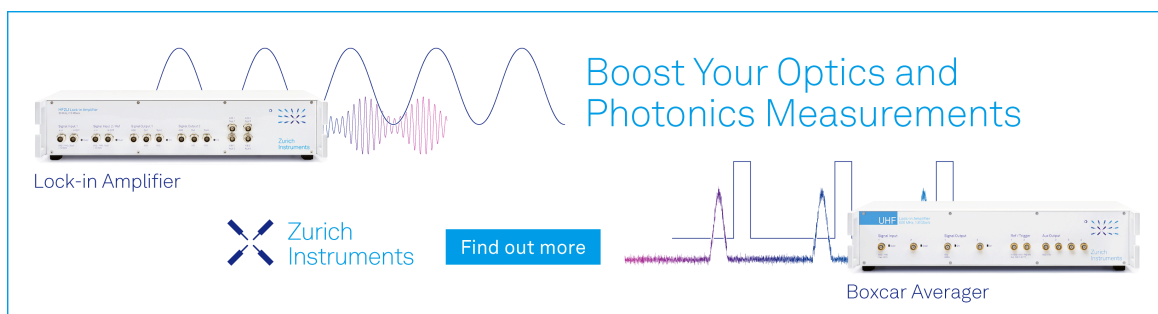R. Cortivo ; J. Campeggio ; M. Zerbetto ✉

Check for updates

View Online   Export Citation

A multiscale approach to coupled nuclear and electronic dynamics. II. Exact and approximated evaluation of nonradiative transition rates

R. Cortivo,[a] (iD) J. Campeggio,[b] (iD) and M. Zerbetto[c] (iD)

AFFILIATIONS

Department of Chemical Sciences, University of Padova, Via Marzolo 1, Padova, Italy

[a] Electronic mail: riccardo.cortivo@phd.unipd.it
[b] Electronic mail: jonathan.campeggio@unifi.it
[c] Author to whom correspondence should be addressed: mirco.zerbetto@unipd.it

ABSTRACT

This work follows a companion article, which will be referred to as Paper I [Campeggio *et al.*, J. Chem. Phys. **158**, 244104 (2023)] in which a quantum-stochastic Liouville equation for the description of the quantum–classical dynamics of a molecule in a dissipative bath has been formulated in curvilinear internal coordinates. In such an approach, the coordinates of the system are separated into three subsets: the quantum coordinates, the classical relevant nuclear degrees of freedom, and the classical irrelevant (bath) coordinates. The equation has been derived in natural internal coordinates, which are bond lengths, bond angles, and dihedral angles. The resulting equation needs to be parameterized. In particular, one needs to compute the potential energy surfaces, the friction tensor, and the rate constants for the nonradiative jumps among the quantum states. While standard methods exist for the calculation of energy and dissipative properties, an efficient evaluation of the transition rates needs to be developed. In this paper, an approximated treatment is introduced, which leads to a simple explicit formula with a single adjustable parameter. Such an approximated expression is compared with the exact calculation of transition rates obtained via molecular dynamics simulations. To make such a comparison possible, a simple sandbox system has been used, with two quantum states and a single internal coordinate (together with its conjugate momentum). Results show that the adjustable parameter, which is an effective decoherence time, can be parameterized from the effective relaxation times of the autocorrelation functions of the conjugated momenta of the relevant nuclear coordinates.

I. INTRODUCTION

In the companion Paper I,[1] a quantum-stochastic Liouville equation (QSLE) in natural internal coordinates (i.e., bond lengths, bond angles, and dihedral angles) has been formulated. The main idea is partitioning of the degrees of freedom (d.o.f.) of the system into three sets: QS, CS, and CB. In QS are included all those coordinates that are relevant to the physical observable under study and need to be treated at the quantum mechanical level. In the QSLE presented in Paper I,[1] only electronic degrees of freedom were considered in this set, even if it can be extended to a few nuclear coordinates. In CS are included the relevant nuclear d.o.f., which are treated explicitly and at the classical level of theory. In particular, the CS coordinates are directly related to the phenomenon under investigation and correspond to the classical environment correlated with the quantum subsystem.[2] Finally, CB includes those nuclear d.o.f. that can be considered irrelevant with respect to the physical observable under study. In the context of the QSLE, the CB coordinates must be (i) fast with respect to CS coordinates and (ii) weakly coupled to the QS coordinates.[3] They represent the dissipative environment of the quantum–classical system. The CB d.o.f. are treated at the classical level and enter in the QSLE implicitly as generators of fluctuation–dissipation on CS coordinates. For this reason, the dynamics of the CS d.o.f. is stochastic.

The QSLE is a set of coupled diffusion-reaction like equations, providing the time evolution of adiabatic electronic populations of the system coupled with nuclear dynamics. The nonadiabatic behavior of the system is described by momentum-jump operators, which allow electronic transitions accompanied by a change in the kinetic energy of the nuclei. The probability of jumping from one electronic state to another depends also upon transition rates (see below), which are functions of the CS coordinates and their conjugated momenta. The set of transition rates is part of the ingredients required to parameterize the QSLE. Apart from the rates, one needs the potential energy surfaces (PESs) of all of the electronic states and the generalized friction tensor as function of the molecular conformation. While standard computational methods exist for the latter two properties, an efficient approach is required for the estimation of transition rates in such a quantum–classical approach.

The calculation of nonadiabatic rates in condensed phases plays a crucial role in the interpretation of nonradiative transition paths and their impact in regard to technological application. Howgate[4] reported the calculation of nonradiative electron transition rates between pure electronic states of Cr^{3+} and V^{3+} in the Al_2O_3 lattice, treating the system as a two-component electron–phonon system and introducing a perturbation Hamiltonian that induces the transitions. A similar approach has been applied to ions doped into insulators or large-gap semiconductors.[5] Another approach that can be found is the application of transition state theory to model the nonradiative rate constant.[6] Therefore, an Arrhenius-like shape is used, with the "activation energy" as the difference in energy for transition from a radiative to a nonradiative state and a pre-exponential constant that is proportional to a frequency of the vibrational mode that is coupled to the transition. The approach is applied to phosphorescent Ir(III) complexes. Mishra and Collins computed radiative and nonradiative rates of polyatomic systems based on the crude adiabatic approximation.[7] The method is suitable for ions in solids. Approaches to compute the nonradiative rates in organic molecules are also found. In the work of Kohn et al.,[8] a heuristic approach that employs machine learning techniques to estimate luminescence quantum yields (and therefore nonradiative rates) reported. In a recent study,[9] a cost-effective method to predict electronic transition rates is introduced and applied to rationalize decay pathways of excited benzophenone. To conclude this short review on the state-of-the-art calculations of nonradiative rates, the work of Egorov et al. should be mentioned.[10] In that work, the authors compute the nonradiative constants of a two-level system that is coupled to a harmonic bath using both a fully quantum mechanical approach and two different classical approaches. The results to suggest that if nonadiabatic relaxation occurs in configurations with small energy gaps, the quantum–classical approach can provide a good approximation to nonradiative rates.

A cost-effective method to compute nonradiative rates in liquid phases, taking into account explicitly nonharmonic nuclear motions, is (to our knowledge) still lacking. In the framework of the quantum–classical Liouville equation (QCLE), Grunwald and Kapral[11] used a modeling approach to compute the transition rates by approximating the bath coordinates as a set of harmonic oscillators. The aim of this work is to provide both a numerical approach to the computation of the transition rates based on classical molecular dynamics simulations and an approximate, yet fast, explicit formula that depends on a single adjustable parameter. A way to guess the

value of such a parameter will be discussed in what follows. We used as test case a simple model system similar to that employed by Grunwald and Kapral as a comparison. In particular, the system consists of two electronic states, coupled to a single nuclear coordinate (and its conjugated momentum) in the CS set. We decided to use a dihedral angle of a simple butane-like model molecule anchored to a surface in order to block the rigid body degrees of freedom.

This paper is organized as follows: In Sec. II, the QSLE is recalled and the exact and approximated approaches to the calculation of the transition rates are introduced. In Sec. III, the transition rates are computed for the model system (which has been described briefly above) and a comparison between the two approaches is discussed. In Sec. IV, conclusive remarks and plans for future work are discussed.

II. METHODOLOGY

A. Quantum-stochastic Liouville equation

The QSLE is a multiscale, nonadiabatic mixed quantum–classical method that describes the stochastic evolution of a system interspersed with transitions among the adiabatic eigenstates. The derivation of the QSLE is reported in the companion Paper I.[1] Here, we report the equation in its final form to make the paper self-consistent. The QSLE is a set of coupled master equations given by

$$\frac{\partial \rho_\alpha(\boldsymbol{\chi}, t)}{\partial t} = -\hat{\Gamma}_{FP}^\alpha(\boldsymbol{\chi}) \rho_\alpha(\boldsymbol{\chi}, t) + \sum_{\beta \neq \alpha}^N m_{\alpha\beta}(\boldsymbol{\chi}) \hat{j}_{\alpha \to \beta}(\boldsymbol{\chi}) \rho_\beta(\boldsymbol{\chi}, t) - m_{\alpha\alpha}(\boldsymbol{\chi}) \rho_\alpha(\boldsymbol{\chi}, t),$$ (1)

where N is the number of electronic states, $\rho_\alpha(\boldsymbol{\chi}, t)$ is the probability density associated with the population of the $\alpha = 1, \ldots, N$ eigenstate, and $\boldsymbol{\chi} = (\mathbf{R}_{CM}, \boldsymbol{\Omega}, \mathbf{q}, \mathbf{P}_{CM}, \mathbf{L}, \mathbf{p}) \equiv (\mathbf{Q}, \boldsymbol{\Pi})$ are the CS nuclear degrees of freedom. In particular, $(\mathbf{R}_{CM}, \mathbf{P}_{CM})$ are respectively the position and momentum of the center of mass, $(\boldsymbol{\Omega}, \mathbf{L})$ are respectively the orientation and angular total angular momentum of the molecule, and $(\mathbf{q}, \mathbf{p})$ are respectively the internal coordinates and their conjugated momenta. $\hat{\Gamma}_{FP}^\alpha(\boldsymbol{\chi})$ is the Fokker–Planck operator of the system that is responsible for the stochastic evolution of $\boldsymbol{\chi}$ on the α-th potential energy surface. The transitions among the PESs are accounted for by the last two terms of Eq. (1). In particular, $m_{\alpha\beta}(\boldsymbol{\chi})$ are the rates of population transfer from β to α, the operator $\hat{j}_{\alpha \to \beta}(\boldsymbol{\chi})$ accounts for the variation of the momenta of the nuclei associated with a transition between two electronic states, while $m_{\alpha\alpha}(\boldsymbol{\chi})$ is the rate for the loss of population of the α state.

The development of an efficient method to evaluate the $m_{\alpha\beta}(\boldsymbol{\chi})$ functions in an ab initio fashion is the objective of the present work.

B. "Exact" calculation of the transition rates

The transition rates for the gain of population are[1]

$$m_{\alpha\beta}(\boldsymbol{\chi}) = \int_0^\infty dt' \int d\boldsymbol{\chi}_B \, M_{\alpha\beta}^{\alpha\beta}(\boldsymbol{\chi}, \boldsymbol{\chi}_B, t') \rho_c(\boldsymbol{\chi}_B | \boldsymbol{\chi}),$$ (2)

where χ_B are the bath d.o.f., $M_{\alpha\beta}^{\alpha\beta}(\chi,\chi_B,t')$ is the memory function, and $\rho_c(\chi_B|\chi)$ is the equilibrium probability density to find the bath d.o.f. in χ_B conditioned by the CS subsystem being in χ. The memory function reads as

$$M_{\alpha\beta}^{\alpha\beta}(\chi,\chi_B,t) = 2\,\mathrm{Re}\big[W_{\alpha\beta}(\chi,\chi_B,t)\big]D_{\alpha\beta}(\chi)D_{\alpha\beta}(\overline{\chi}_{\alpha\beta,t}), \quad (3)$$

where

$$W_{\alpha\beta}(\chi,\chi_B,t) = e^{-i\int_t^0 d\tau\,\omega_{\alpha\beta}(\overline{\mathbf{Q}}_{\alpha\beta,\tau})}, \quad (4)$$

$$D_{\alpha\beta}(\chi) = \mathbf{g}\cdot\mathbf{p}'\cdot\mathbf{d}_{\alpha\beta}^{\mathrm{INT}}(\mathbf{Q}), \quad (5)$$

$$\omega_{\alpha\beta}(\mathbf{Q}) = \big[E_\alpha(\mathbf{Q},\mathbf{Q}_B) - E_\beta(\mathbf{Q},\mathbf{Q}_B)\big]/\hbar, \quad (6)$$

$$\mathbf{p}' = \mathbf{A}\cdot\mathbf{L} + \mathbf{p}, \quad (7)$$

where $E_\alpha(\mathbf{Q},\mathbf{Q}_B)$ is the PES in the electronic state α, $\mathbf{g}$ and $\mathbf{A}$ are, respectively, the contravariant tensor and the Gauge potential matrix,[12] $\mathbf{d}_{\alpha\beta}^{\mathrm{INT}}(\mathbf{Q})$ is the nonadiabatic coupling vector, and $\overline{\chi}_{\alpha\beta,t}$ represents the time-reversed trajectory of the system after transition from E_α to the average PES $E_{\alpha\beta} = (E_\alpha + E_\beta)/2$.

In Eq. (2), two integrals appear. The first one is to be carried out over the bath d.o.f., while the second integral is carried out over time. As suggested in the work of Grunwald and Kapral,[11] the former integral can be replaced by the average over an ensemble of trajectories on $E_{\alpha\beta}$,

$$\int d\chi_B\, M_{\alpha\beta}^{\alpha\beta}(\chi,\chi_B,t)\rho_c(\chi_B|\chi) = \frac{1}{N_\chi}\sum_{i=1}^{N_\chi} M_{\alpha\beta,i}^{\alpha\beta}(\chi,\chi_B,t), \quad (8)$$

where N_χ is the number of molecular dynamics trajectories that in a period of time t are found in χ, and $M_{\alpha\beta,i}^{\alpha\beta}(\chi,\chi_B,t)$ is the memory function computed using the i-th trajectory. The key idea of Eq. (8) is that the average over the N_χ ensemble of trajectories is an average over the conditional probability density $\rho_c(\chi_B|\chi)$. The equivalence is valid in the limit $N_\chi \to \infty$.

The computation of transition rates as expressed in Eq. (8) is very resource demanding as it will be shown in Sec. III A. It becomes infeasible rapidly with the dimensions of χ. For this reason, a fast (even if approximated) approach is desirable.

C. Approximated explicit formula for the transition rates

Here, an approximated explicit formula is introduced for the calculation of transition rates. The basic idea shares some assumptions with the approach proposed by Rank and Kapral.[13] The main difference is that our derivation does require to model the $\rho_c(\chi_B|\chi)$ probability density (which for simplicity is usually shaped as a multivariate Gaussian, i.e., the bath is considered harmonic). The derivation presented in this subsection is based on the high-friction limit, on the fast relaxation of the bath phase-space coordinates, and on the weak interaction between CB and CS degrees of freedom. Therefore, the method presented here is suitable to describe the quantum–classical dynamics of a molecule in liquid phase.

Under these conditions, the memory function $M_{\alpha\beta,i}^{\alpha\beta}(\chi,\chi_B,t)$ is expected to show a short time decay with respect to the timescale of the dynamics of χ. It is useful to rewrite Eq. (3) by making explicit both the phase factor and the time-reversed evolution. The memory function reads

$$M_{\alpha\beta}^{\alpha\beta}(\chi,\chi_B,t) = 2\,\mathrm{Re}\Big[e^{-i\int_t^0 d\tau\,e^{-iL_{\alpha\beta}(\overline{\chi}_{\alpha\beta},\chi_B)\tau}\omega_{\alpha\beta}(\mathbf{Q})}\Big]$$
$$\times D_{\alpha\beta}(\chi)e^{-i\hat{L}_{\alpha\beta}(\overline{\chi}_{\alpha\beta},\chi_B)t}D_{\alpha\beta}(\overline{\chi}_{\alpha\beta}), \quad (9)$$

where $i\hat{L}_{\alpha\beta}(\overline{\chi}_{\alpha\beta},\chi_B)$ is the Liouville operator associated with the classical evolution on $E_{\alpha\beta}$. Such an energy difference term can be split into a zero-order term that depends only on CS, i.e., $E_{\alpha\beta}^{(0)}(\mathbf{Q})$, a term that depends only on bath coordinates, i.e., $E_{\alpha\beta}^{(B)}(\mathbf{Q}_B)$, and an interaction term, $E_{\alpha\beta}^{(\mathrm{int})}(\mathbf{Q},\mathbf{Q}_B)$ such that

$$E_{\alpha\beta}(\mathbf{Q},\mathbf{Q}_B) = E_{\alpha\beta}^{(0)}(\mathbf{Q}) + E_{\alpha\beta}^{(B)}(\mathbf{Q}_B) + E_{\alpha\beta}^{(\mathrm{int})}(\mathbf{Q},\mathbf{Q}_B). \quad (10)$$

Moreover, due to the assumption of weak coupling between CS and CB d.o.f., the total nuclear kinetic energy can be written as

$$K(\overline{\chi}_{\alpha\beta},\chi_B) \approx K^{(0)}(\overline{\chi}_{\alpha\beta}) + K^{(B)}(\chi_B). \quad (11)$$

When Eqs. (10) and (11) are substituted into the expression of the Liouville operator $i\hat{L}_{\alpha\beta}(\overline{\chi}_{\alpha\beta},\chi_B)$, the latter can in turn be split into

$$i\hat{L}_{\alpha\beta}(\overline{\chi}_{\alpha\beta},\chi_B) = i\hat{L}_{\alpha\beta}^{(0)}(\overline{\chi}_{\alpha\beta}) + i\hat{L}_{\alpha\beta}^{(\mathrm{int})}(\overline{\chi}_{\alpha\beta},\chi_B) + i\hat{L}^{(B)}(\chi_B), \quad (12)$$

where

$$i\hat{L}_{\alpha\beta}^{(\mathrm{int})}(\overline{\chi}_{\alpha\beta},\chi_B) = -\nabla_{\mathbf{Q}}E_{\alpha\beta}^{(\mathrm{int})}(\mathbf{Q},\mathbf{Q}_B)\cdot\big(\nabla_{\overline{\mathbf{\Pi}}_{\alpha\beta}} - \nabla_{\mathbf{\Pi}_B}\big). \quad (13)$$

Since the averaging of the memory function is expected to be a fast process with respect to the nuclear dynamics, the Suzuki–Trotter expansion is applied here to obtain

$$e^{-iL_{\alpha\beta}(\overline{\chi}_{\alpha\beta},\chi_B)t} \approx e^{-i\hat{L}_{\alpha\beta}^{(0)}(\overline{\chi}_{\alpha\beta})t}e^{-i\hat{L}_{\alpha\beta}^{(\mathrm{int})}(\overline{\chi}_{\alpha\beta},\chi_B)t - i\hat{L}^{(B)}(\chi_B)t}, \quad (14)$$

which can be used to recast the integral over bath coordinates in Eq. (9) to

$$\int d\chi_B\, M_{\alpha\beta}^{\alpha\beta}(\chi,\chi_B,t)\rho_c(\chi_B|\chi)$$
$$\approx 2\,\mathrm{Re}\Big[e^{-i\int_t^0 d\tau\,e^{-iL_{\alpha\beta}^{(0)}(\overline{\chi}_{\alpha\beta})\tau}\omega_{\alpha\beta}(\mathbf{Q})}\Big]$$
$$\times D_{\alpha\beta}(\chi)e^{-i\hat{L}_{\alpha\beta}^{(0)}(\overline{\chi}_{\alpha\beta})t}\Big[\big(\mathbf{g}^{\mathrm{T}}\mathbf{d}_{\alpha\beta}^{\mathrm{INT}}(\mathbf{Q})\big)\cdot$$
$$\cdot\int d\chi_B\,\rho_c(\chi_B|\chi)e^{-i\hat{L}_{\alpha\beta}^{(\mathrm{int})}(\overline{\chi}_{\alpha\beta},\chi_B)t - i\hat{L}^{(B)}(\chi_B)t}\overline{\mathbf{P}}_{\alpha\beta}'\Big], \quad (15)$$

where $\mathbf{d}_{\alpha\beta}^{\mathrm{INT}}(\mathbf{Q})$ is the conformational part of the diabatic coupling vector.[1]

The average of memory function is therefore rewritten as a product of a function that, despite its complexity, depends only on CS coordinates multiplied by a function that is the average over the conditional Boltzmann probability density of the bath coordinates $(\rho_c(\chi_B|\chi))$ of the possible shifts in momenta conjugated to the CS

coordinates. The last integral in Eq. (15) is a function that decays in time due to randomization of the velocities.[13]

The next step is to bypass the calculation of bath integral, by introducing the ansatz

$$e^{-\tau_{\text{dec}}^{-1} t} \, \overline{\mathbf{P}}'_{\alpha\beta} \approx \int d\chi_B \, \rho_c(\chi_B|\chi)$$
$$\times e^{-i\hat{L}_{\alpha\beta}^{(\text{int})}(\overline{\chi}_{\alpha\beta},\chi_B)t - i\hat{L}^{(B)}(\chi_B)t} \, \overline{\mathbf{P}}'_{\alpha\beta}, \quad (16)$$

where τ_{dec} is assumed to be a diagonal matrix, each element of which represents an effective decoherence time for each of the momenta conjugated to the internal coordinates $\mathbf{q}$. A justification for Eq. (16) is provided in Appendix A.

Substituting Eq. (16) into Eq. (15), the transition rates can be expressed as

$$m_{\alpha\beta}(\chi) \approx \int_0^\infty dt' \, \tilde{M}_{\alpha\beta}^{\alpha\beta}(\chi, t'), \quad (17)$$

where

$$\tilde{M}_{\alpha\beta}^{\alpha\beta}(\chi, t) = 2 \, \text{Re}[\tilde{W}_{\alpha\beta}(\chi, t)] D_{\alpha\beta}(\chi) \tilde{D}_{\alpha\beta}(\overline{\chi}_{\alpha\beta, t}), \quad (18)$$

$$\tilde{W}_{\alpha\beta}(\chi, t) = \exp\left[-i \int_t^0 d\tau \, e^{-i\hat{L}_{\alpha\beta}^{(0)}(\overline{\chi}_{\alpha\beta})\tau} \omega_{\alpha\beta}(\mathbf{Q})\right], \quad (19)$$

$$\tilde{D}_{\alpha\beta}(\overline{\chi}_{\alpha\beta}) = \left[e^{-\tau_{\text{dec}}^{-1} t} \, \mathbf{g}^{\text{T}} \mathbf{d}_{\alpha\beta}^{\text{INT}}(\mathbf{Q})\right] \cdot \left[e^{-i\hat{L}_{\alpha\beta}^{(0)}(\overline{\chi}_{\alpha\beta})t} \, \overline{\mathbf{P}}'_{\alpha\beta}\right]. \quad (20)$$

Since the computation of Eq. (17) does not require knowledge of $\rho_c(\chi_B|\chi)$, and the integral has substituted with a simple exponential expression, the computational cost is orders of magnitude smaller than the exact protocol presented above. The price to pay is that a set of adjustable parameters, i.e., the diagonal elements of the τ_{dec} matrix, are introduced. A possible strategy to parameterize the decoherence time is provided in what follows.

D. Estimation of the decoherence times

The exponential decay matrix $e^{-\tau_{\text{dec}}^{-1} t}$ introduced in Eq. (16) is a simple way to model the effect of bath coordinates on transition rates, which is to make the system lose memory of its initial configuration. As it has been observed by Rank and Kapral,[13] the decoherence time is smaller the higher the friction is. It can be expected that τ_{dec} can be estimated from time autocorrelation function of the momenta. In the Sec. III, the goodness of such an assumption is proven for a Lennard-Jones solvent.

The autocorrelation function of the momenta can be computed from an all-atom molecular dynamics simulation carried out on the average PES $E_{\alpha\beta}(\mathbf{Q}, \mathbf{Q}_B)$ and taking as $\tau_{\text{dec},i}$ the time at which the autocorrelation function of the momentum p_i is equal to e^{-1}. While such a procedure would be very simple in Cartesian coordinates, some additional work is required in internal coordinates since the metric tensor $\mathbf{g}$ must be used.[12] A second, simpler route can be followed if $E_{\alpha\beta}$ presents a single minimum. The autocorrelation function of the momentum conjugated to the i-th coordinate can be modeled as

$$C_i(t) = \frac{\lambda_{+,i}^2}{\lambda_{+,i}^2 - k_i/g_i} e^{-\lambda_{+,i} t} - \frac{k_i/g_i}{\lambda_{+,i}^2 - k_i/g_i} e^{-\lambda_{-,i} t}, \quad (21)$$

where

$$\lambda_{\pm,i} = \frac{\xi_i}{2g_i} \pm \frac{1}{2}\sqrt{\frac{\xi_i^2}{g_i^2} - 4\frac{k_i}{g_i}}, \quad (22)$$

while ξ_i, g_i, and k_i are respectively the i-th diagonal elements of the friction, covariant, and curvature matrices associated with the i-th internal coordinate q_i, respectively, whose average PES is locally approximated by the harmonic potential

$$E_{\alpha\beta}(q_i) \approx \frac{1}{2}k_i(q_i - q_{i,\text{eq}})^2. \quad (23)$$

A detailed derivation of Eq. (21) is provided in Appendix B.

E. Model system

In Sec. II, two methods to compute the transition rates have been introduced. The "exact" method provides a way to compute the integral over bath coordinates using MD simulations. However, it becomes unfeasable as soon as a few internal degrees of freedom are included in the CS set. The second approach is based on the assumption of weak (energetic) coupling between the CS and CB coordinates, and on the fast loss of memory with respect to the time evolution of both the populations (QS d.o.f.) and the CS degrees of freedom. Such an approximated approach requires limited computational effort with respect to the exact protocol. To test the validity of the approximated method, the transition rates are here estimated using both the approaches presented in the previous subsections on a test-case model system. The objective is to test the approximated method on a model system that resembles the molecular systems target of the approach presented here, i.e., flexible molecules in liquids. It is worth noting that the model system is intended to benchmark the approximations that, in a dissipative environment, lead to the QSLE and to benchmark the approximated estimation of the transition rates. A system similar to that used by Grunwald and Kapral was chosen,[11] i.e., the quantum–classical system is described by a single nuclear coordinate (CS) and two electronic states (QS), immersed in a classical (stochastic) dissipative bath (CB).

In detail, the model system (represented in Fig. 1) is built by a coarse-grained molecule composed of four beads with a butane-like topology. The bond lengths are fixed to 2.5 Å, and the bond angles are fixed to 120°, so that the only internal degree of freedom is the dihedral angle. The molecule is anchored to a surface made of 50 dummy atoms ($\varepsilon = -0.12$ kcal/mol and $R_{\text{min}} = 3.4$ Å), which are kept fixed. Such a surface is blocking the translation and rotation of the molecule. Apart from this constraint, there is no potential energy interaction between the anchor points of the surface and the four-bead molecule. Finally, the system is immersed in 330 solvent molecules treated at a coarse-grained level as single beads. The MARTINI force field was employed to parameterize the Lennard-Jones potential. In particular, type IV beads were used for the solute,[14] and MARTINI water parameters were used for the solvent.[15] An example conformation of the model system is provided in Fig. 1. The relevant nuclear d.o.f. are therefore $\chi = (\varphi, p_\varphi)$ with φ the dihedral angle and p_φ its conjugated momentum.
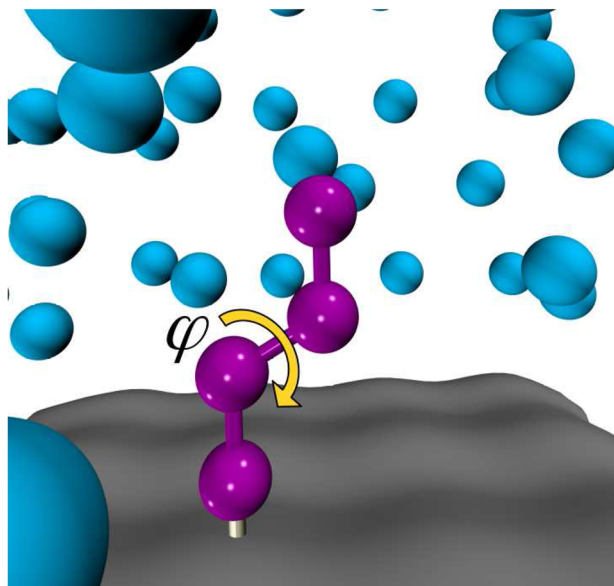
FIG. 1. Representation of the model system. The coarse-grained molecule is represented by purple spheres connected by sticks. The cyan spheres represent the water beads, and the gray plane represents the surface that serves as anchor point for the molecule. The yellow curved arrow highlights the unique internal degree of freedom included in the model, i.e., the dihedral angle φ.
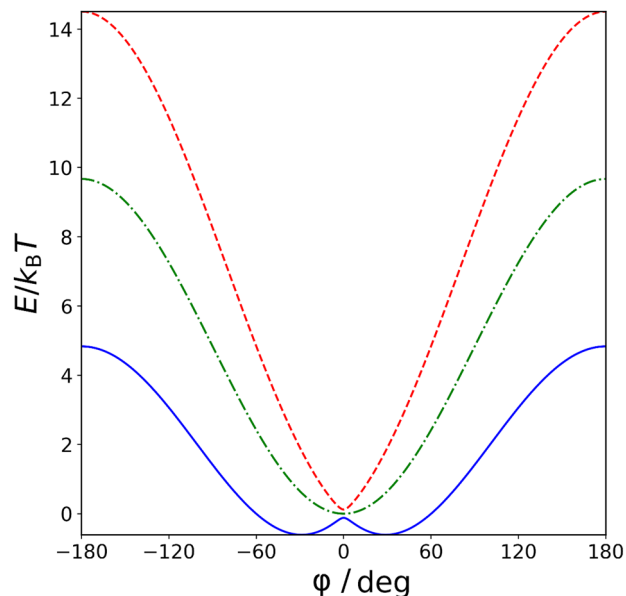

FIG. 2. Plot of the PESs as functions of the dihedral angle for $V_0 = 4.835 k_B T$, $\Delta = 1.0$, and $\delta = 0.025$. Blue solid line E_0, red dashed line E_1, green dotted-dashed line the average surface E_{01}.

A two-level system is considered, where, for example, the electronic states can be HOMO (0) and LUMO (1) energy levels. Therefore, the QSLE consists of just two coupled partial differential equations, given by

$$\begin{cases} \dfrac{\partial \rho_0(\boldsymbol{\chi}, t)}{\partial t} = -\hat{\Gamma}_{FP}^0 \rho_0(\boldsymbol{\chi}, t) + m_{01}(\boldsymbol{\chi}) \rho_1(\bar{\bar{\chi}}_{01}, t) - m_{00}(\boldsymbol{\chi}) \rho_0(\boldsymbol{\chi}, t), \\ \dfrac{\partial \rho_1(\boldsymbol{\chi}, t)}{\partial t} = -\hat{\Gamma}_{FP}^1 \rho_1(\boldsymbol{\chi}, t) + m_{10}(\boldsymbol{\chi}) \rho_0(\bar{\bar{\chi}}_{10}, t) - m_{11}(\boldsymbol{\chi}) \rho_1(\boldsymbol{\chi}, t), \end{cases} \tag{24}$$

where $\bar{\bar{\chi}}_{\alpha\beta} = \hat{j}_{\alpha \to \beta}(\boldsymbol{\chi})\boldsymbol{\chi}$, and the Fokker–Planck operator of the $\alpha = 0, 1$ state $\hat{\Gamma}_{FP}^\alpha$ reads

$$\hat{\Gamma}_{FP}^\alpha = \frac{p_\varphi}{g_\varphi} \frac{\partial}{\partial \varphi} + F_\alpha(\varphi) \frac{\partial}{\partial p_\varphi} - \frac{\partial}{\partial p_\varphi} \xi_\varphi \frac{p_\varphi}{g_\varphi} - k_B T \frac{\partial}{\partial p_\varphi} \xi_\varphi \frac{\partial}{\partial p_\varphi}, \tag{25}$$

where $F_\alpha(\varphi)$ is the Hellmann–Feynman force

$$F_\alpha(\varphi) = -\frac{\partial E_\alpha(\varphi)}{\partial \varphi}, \tag{26}$$

g_φ is the conformational element of the covariant metric tensor,[12] and ξ_φ is the conformational part of the friction tensor. The latter could be parameterized via a hydrodynamic approach.[16]

To obtain the PESs, a model Hamiltonian has been employed, taking as representation of the potential energy (**V**) over the two electronic states the matrix

$$\mathbf{V} = V_0 \begin{bmatrix} \Delta - \cos\varphi + \sin(\varphi/2) & -\delta \\ -\delta & \Delta - \cos\varphi - \sin(\varphi/2) \end{bmatrix}, \tag{27}$$

where V_0 is a scaling factor of the potential, Δ is an energy shift common to all the eigenvalues, and δ regulates the energy separation between the electronic levels. Both Δ and δ are dimensionless quantities, while V_0 has the dimension of energy. Such a representation leads to PESs that resemble those employed by Grunwald and Kapral[11] in their work. In all the calculations, $V_0 = 4.835 k_B T$, $\Delta = 1.0$, and $\delta = 0.025$. The resulting eigenvalues are

$$\begin{cases} E_0(\varphi) = V_0 \left[\Delta - \cos\varphi - \sqrt{\delta^2 + \sin^2(\varphi/2)} \right], \\ E_1(\varphi) = V_0 \left[\Delta - \cos\varphi + \sqrt{\delta^2 + \sin^2(\varphi/2)} \right]. \end{cases} \tag{28}$$

The two PESs are shown in Fig. 2, along with the mean PES $E_{01}(\varphi)$.

The nonadiabatic vectors computed from the eigenfunctions of **V** become scalar functions of the dihedral angle, $d_{01}(\varphi)$ and $d_{10}(\varphi)$. These coefficients provide the propensity for nonadiabatic events to occur. In fact, as it is shown in Fig. 3, $d_{01}(\varphi)$ reaches its peak for $\varphi = 0$, where the energy gap between E_0 and E_1 is minimum.

III. RESULTS

A. "Exact" protocol

The exact computation of transition rates is very resource demanding, since it requires an ensemble of trajectories of the system [Eq. (8)] large enough to sample the conditional Boltzmann distribution of the bath coordinates in each point of the phase-space of CS. In this case, the molecular dynamics simulations were performed using NAMD software,[17,18] at 300 K with a fixed box 25.845 × 26.16 × 60 Å^3. Since 300 MD trajectories have been required to compute Eq. (8) in the (φ, p_φ) phase space (see below), we decided to run canonical NVT simulations instead of NVE, for which a
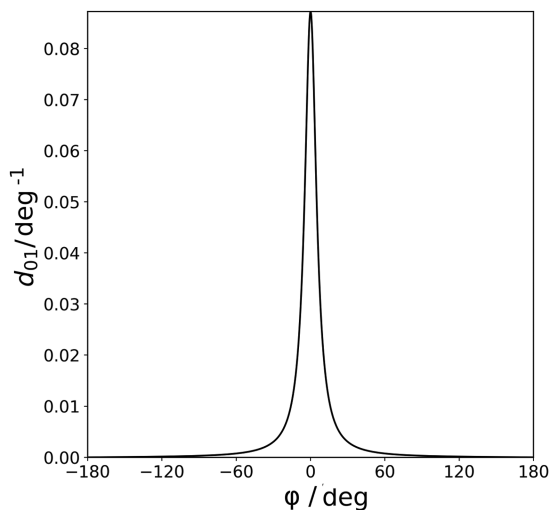
FIG. 3. Plot of the nonadiabatic coupling d_{01} as function of the dihedral angle for $V_0 = 4.835 k_B T$, $\Delta = 1.0$, and $\delta = 0.025$.

larger simulation box would have been needed, thus increasing the computational time. The Langevin thermostat has been employed with a correlation time of 0.2 ps, which ensures correct calculation of the self-diffusion coefficient of water,[17] thus assuming that the dynamical properties of the solute are reliable. The time step was set to 1 fs, and periodic boundary conditions were applied in all directions (assuming that because of the short-range behavior of the Lennard-Jones potential, the interaction among solvent beads above and below the dummy atoms surface was negligible). The Colvars[19] package of NAMD was employed to extract the dihedral angle time series.

The function $m_{01}(\chi)$ was obtained over a discrete grid in the (φ, p_φ) phase space. In particular, the selected bin widths were $\Delta \varphi = 0.5°$, and $\Delta p_\varphi = 0.05(g_\varphi k_B T)$, which were chosen in such a way that both energy and nonadiabatic coupling do not change abruptly within the bins. The domain was limited to $-6.0° < \varphi < +6.0°$ and $0.5 < p_\varphi/(g_\varphi k_B T)^{1/2} < 2.0$, which is the region where, at 300 K and given the shape of the PESs, it is expected to mostly find the system and, therefore, where it will be mostly probable to observe a jump between the two electronic states. For larger values of $|\varphi|$, the transition rate rapidly tends to zero because the nonadiabatic coupling drops (see Fig. 3). For large values of $|p_\varphi|$, one should expect the system to have more energy to promote the electronic transition, but the probability of finding the system with such a high kinetic energy drops exponentially to zero.

The MD protocol was as follows: First, a preliminary long trajectory of 52 ns saving coordinates each 1 ps was computed (discarding the first 2 ns as equilibration time). Such a trajectory serves to sample the average PES, E_{01}. Second, 300 equally distributed configurations were extracted from the long trajectory and used as starting points for short, 6 ns trajectories (discarding the first 0.5 ns as equilibration time), saving coordinates each 1 fs. The third step was to split each of the short trajectories into small chunks of 0.5 ps. Based on the final value of (φ, p_φ), a chunk of trajectory is assigned to one bin in the grid defined above. For example, a chunk of trajectory

ending at $\chi|_{t=0.5\text{ps}} = (\varphi = 0.12°, p_\varphi = -1.34(g_\varphi k_B T)^{1/2})$ is assigned to the bin $(0.0° < \varphi < 0.5°, -1.35 < p_\varphi/(g_\varphi k_B T)^{1/2} < -1.30)$. In this step, N_χ trajectories for each bin were collected [see Eq. (8)].

The fourth step was the computation of the i-th memory function, $M_{01,i}^{01}(\chi, \chi_B, t)$ at each time step, for the N_χ chunks belonging to each bin, followed by calculation of the mean value as expressed in Eq. (8). The resulting bath average was significantly affected by the value of N_χ. In particular, the higher the value of N_χ, the smaller was the noise of the average memory function.

The last step was comprised of numerical integration over time of the average memory functions. The integration should be performed until the integrating function decays to zero. However, because of low statistics for some of the bins, the tails of memory functions were too noisy. In these cases, the upper integration extreme was set at 0.5 ps, which was the total length of a chunk. A schematic representing the protocol defined above is shown in Fig. 4.

As mentioned above, this approach is very resource demanding and it becomes rapidly infeasible as soon as the dimension of
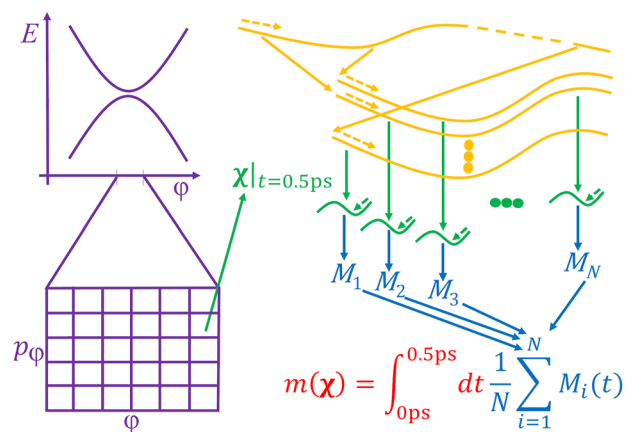

FIG. 4. Visual representation of the exact protocol to compute $m_{01}(\chi)$. The colors are associated with the five steps described in the main text, following the order violet → orange → green → blue → red.
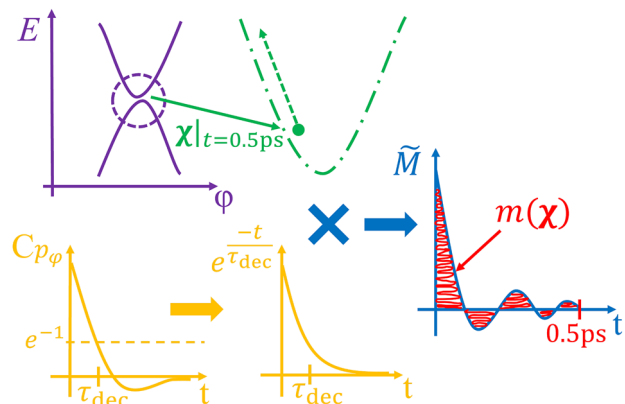

FIG. 5. Visual representation of the approximate protocol to compute $m_{01}(\chi)$. The colors are associated with the five steps described in the main text, following the order violet → green → orange → blue → red.

χ increases to just a few coordinates. For example, if the CS set contains two internal coordinates, the sampling on the adiabatic dynamics must be done in four directions (two for the coordinates and two for their conjugated momenta), making the number of short trajectories increase exponentially to ensure a statistically large N_χ value. For this reason, a faster, even if approximated, estimation of the rate coefficients is desirable.

B. Approximated protocol

The protocol used to compute the approximated transition rates can be divided into five steps. The first one was the selection of φ and p_φ domains with the highest transition probability

that were the same as defined in the exact protocol. The best way to select the extent of φ and p_φ is to consider only the domain in which $\Delta E_{01} > E_k$, where the last term represents the kinetic energy associated with the system d.o.f. In this way, all the configurations without enough energy to overcome the barrier potential are cut out. Then, the resulting domain has to be compared with the nonadiabatic coupling, excluding the region where d_{01} is too small to provide population transfer.

The second step was computation of the "fictitious" time-reversed trajectory. In other words, the Newton dynamics along $E_{01}(\varphi)$ was simulated without the influence of bath degrees of freedom. In this way, a single trajectory was computed, instead of hundreds, needed in the exact protocol.
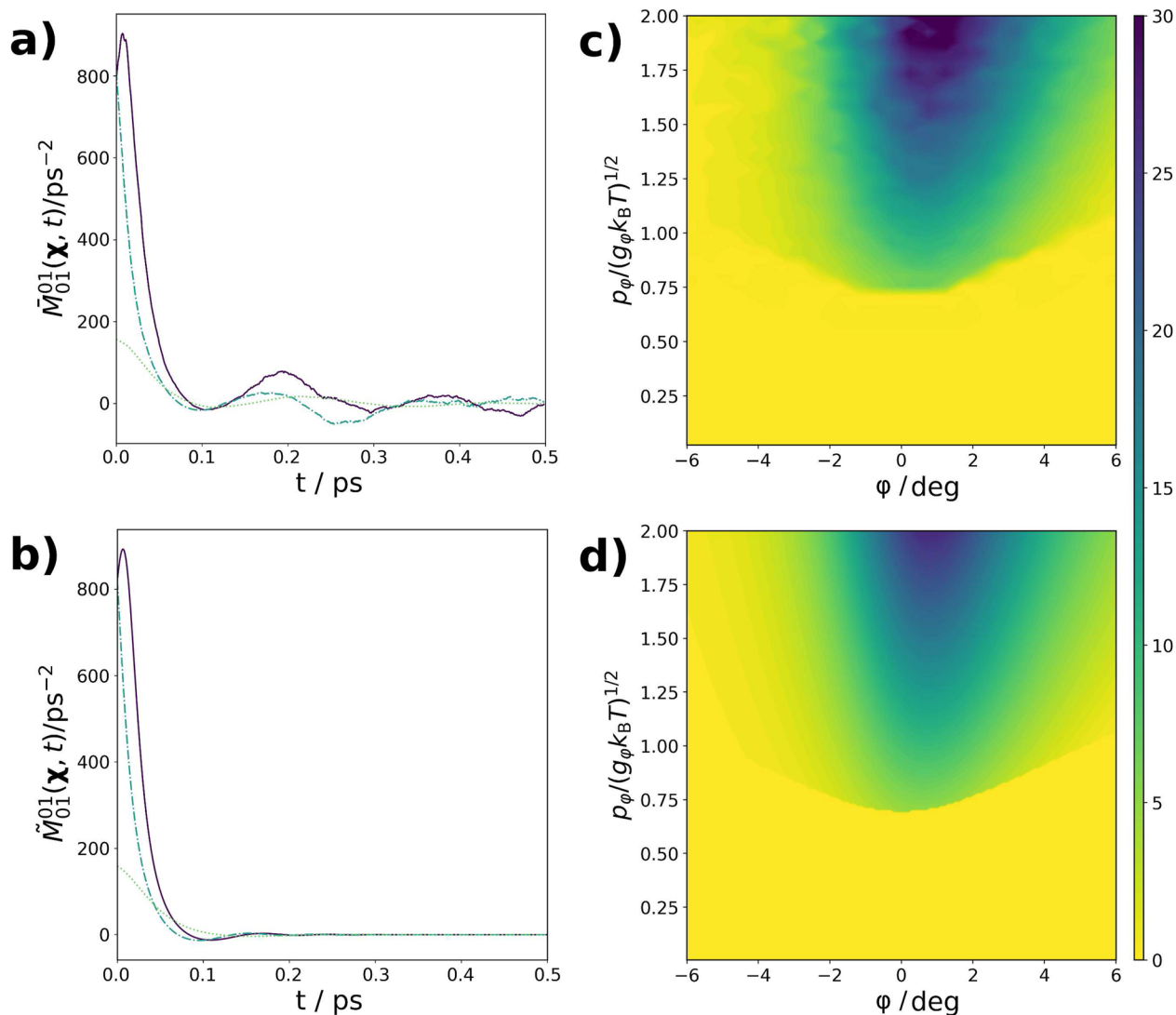

FIG. 6. (a) Plot of the bath average of the memory function computed via the exact protocol for different grid points: violet solid line, $\chi = (1.2°, 2.00(g_\varphi k_B T)^{1/2})$; light blue dotted-dashed line, $\chi = (-1.2°, 2.00(g_\varphi k_B T)^{1/2})$; light green dotted line, $\chi = (0.2°, 0.82(g_\varphi k_B T)^{1/2})$. (b) Plot of the bath average of the memory function computed via the approximate protocol for different grid points: violet solid line, $\chi = (1.2°, 2.00(g_\varphi k_B T)^{1/2})$; light blue dotted-dashed line, $\chi = (-1.2°, 2.00(g_\varphi k_B T)^{1/2})$; light green dotted line, $\chi = (1.2°, 0.82(g_\varphi k_B T)^{1/2})$. (c) Surface plot of exact $m_{01}(\varphi, p_\varphi)$ in ps^{-1}. (d) Surface plot of approximate $m_{01}(\varphi, p_\varphi)$ in ps^{-1}.

The third step consisted of computing the decaying exponential $e^{-t/\tau_{dec}}$. For this purpose, the approximate autocorrelation function of p_φ was computed [Eq. (21)], and τ_{dec} was chosen as the time at which the function was equal to $1/e$.

The fourth step consisted of computing the product between backward trajectories and the decaying exponential to obtain $\tilde{M}_{01}^{01}(\chi, t)$. This step was much faster compared to the corresponding step of the exact protocol.

Finally, the transition rate was obtained by time integration. Since the integral was not analytical, the Euler forward integration method was performed, using a time step of 0.1 fs. The upper extreme of the integral t_d was fixed at 0.5 ps, as it was set in the exact protocol. A schematic representing the protocol is shown in Fig. 5.

C. Discussion

Figures 6(a) and 6(b) show comparison between the exact ($\bar{M}_{01}^{01}(\chi, t)$) and the approximated ($\tilde{M}_{01}^{01}(\chi, t)$) bath average of the memory function associated with the relaxation from the excited state to the ground state $m_{01}(\chi)$, at three different points in the χ phase space.

As it can be seen below, the approximated protocol reproduces the exact functions quite well, even though it shows a larger damping of the tail oscillations. However, it is difficult to say whether this is a problem of the approximated protocol or an effect of low statistics in the exact protocol.

Figures 6(c) and 6(d) show comparison between the exact and the approximated transition rates. Both the trends and the absolute values of $m_{01}(\chi)$ are well reproduced from the approximated approach. In particular, the higher the momentum, the higher the transition rate, due to the greater nuclear kinetic energy that can be converted into electronic potential. Along the dihedral angle, instead, the transition rate increases as φ tends to zero, as it was expected from the shape of the nonadiabatic coupling term (Fig. 3). In addition, it appears that the function is not symmetric around $\varphi = 0°$. Since the configurations explored during a time-reversed trajectory depend on the starting value of χ, for a positive value of the momentum, it is generally true that $\varphi(t - \Delta t) < \varphi(t)$ (and an analogous observation holds for a negative momentum, inverting the inequality). Therefore, since d_{01} is symmetric around $0°$, the asymmetry in probability of the time-reversed trajectories is translated into a larger transition rate for $\varphi > 0°$.

IV. CONCLUSIONS

The results reported in this paper (i) show that a dissipative bath implies fast relaxation of the memory kernel of jumps among PESs, and the timescale allows one to determine whether or not the Markovian approximation can be done; (ii) because of the high-friction limit in condensed phases, a cost-effective explicit formula for the calculation of the transition rates can be obtained.

The first observation is a partial benchmark of the method. The difficulties to benchmark the QSLE by comparison to a full quantum mechanical calculation arise from the necessity for computing the quantum dynamics of a large number of molecules (e.g., here 300 beads were used to simulate the solvent) that interact with each other and with the relevant part of the system (the solute) with a Lennard-Jones (or, in general, nonbonded) interaction. Usually, the 1D simple avoided crossing model introduced by Tully[20] is used as a benchmark for quantum–classical methods, but such a model is not suited for the QSLE since there is no dissipative environment. This, in turn, breaks the Markovian nature of jumps among the PESs. The Markovian approximation can be easily substituted by a non-Markovian time evolution of the quantum subsystem and in the absence of a dissipative bath, the QSLE is just a QCLE, which has been already benchmarked against the Tully model with satisfying results.[2] In literature, a benchmark of the performance of harmonic and nonharmonic classical baths in quantum–classical descriptions has been attempted,[10] but using this work as a benchmark for the QSLE is not directly possible because the quantum–classical models are in part different and since the authors of that work are mostly interested in dynamics in solids. Further work is required to try to benchmark the QSLE with a full quantum calculation. At least, in this paper it was tested that a dissipative environment implies fast relaxation of the memory functions due to bath averaging, as it was shown in Figs. 6(a) and 6(b). The results also provide a limit to the characteristic timescale of the QS and CS d.o.f. in order to assume the Markovian dynamics and this timescale seems to be linked to the relaxation of the CS momenta.

The second result is the approximated, but cost-effective, protocol to estimate the transition rates for jumps among electronic PESs. At the basis of the approximation is the fast relaxation dynamics of the bath degrees of freedom, allowing linearization of the exponential operators entering in the expression for rates. The final formula, i.e., Eq. (17) (and equations below), requires the calculation of a classical molecular dynamics trajectory on the average PES. Note that Eqs. (17) and (18) are computed on the time-reversed evolution of the relevant coordinates in vacuum. Equation (17) relies on a free parameter, which has been called an effective decoherence time. It is responsible for the loss of memory in the master equation part of the QSLE. Therefore, it represents the timescale characteristic for the jump from the actual PES to another one, independent of which path among PESs was followed earlier. Such a single parameter was introduced as an ansatz in place of the very complex integral to be carried out in the coordinates and momenta of the bath coordinates. Such an integral is unfeasible both for the high dimensionality of the bath phase space and for the complicated expression of the integrand function. While a free parameter is introduced, the shape of the integrand suggests that the decoherence time is related to the relaxation of the conjugated momenta of the relevant degrees of freedom. Therefore, given that the relevant dynamics in the average PES is the vibration around the energy minimum, we were able to compute analytically the relaxation time for the momentum and it turned out to be in the correct order of magnitude. If anharmonicity is not negligible, such a correlation time can be computed from short molecular dynamics simulations.

Two steps are planned as further work. First, the implementation of a numerical method to solve the QSLE, in particular to have access to the time evolution of the electronic populations coupled with the motions of nuclei. Such a work is in progress and the method chosen for the numerical solution is the local radial basis function collocation approach.[21–23] It is a meshfree protocol that should allow to solve the QSLE in a multidimensional coordinate space.

The second step is the application of the QSLE to study the relaxation pathways of excited organic molecules in liquid phases. Evidence has shown that conformational changes of the molecule—in particular the timescales of nuclear motions—can affect such a pathway.[9] The QSLE provides the perfect framework to include the relevant dynamics of nuclei in the dynamics of electronic populations. To pursue this objective, a choice will have to be made on how the PESs will be calculated and treated. In the present formulation, the QSLE does not include relaxation due to intersystem crossing if the PESs are pure spin states. Therefore, further work is required to provide a way to include the ISC mechanism in the model.

ACKNOWLEDGMENTS

AUTHOR DECLARATIONS

Conflict of Interest

The authors have no conflicts to disclose.

Author Contributions

R. Cortivo: Conceptualization (equal); Data curation (equal); Formal analysis (equal); Investigation (equal); Methodology (equal); Validation (equal); Visualization (equal); Writing – original draft (equal). **J. Campeggio**: Data curation (equal); Formal analysis (equal); Methodology (equal); Validation (equal); Visualization (equal). **M. Zerbetto**: Conceptualization (equal); Methodology (equal); Project administration (equal); Supervision (equal); Visualization (equal); Writing – review & editing (equal).

DATA AVAILABILITY

The data that support the findings of this study are available within the article.

APPENDIX A: EXPONENTIAL ASSUMPTION

In this appendix, a qualitative explanation of Eq. (16) is provided. In order to simplify the bath integral in Eq. (15), the following Taylor expansion is performed:

$$e^{-i\hat{L}_{\alpha\beta}^{(\text{int})}(\overline{\chi}_{\alpha\beta},\chi_{\text{B}})t - i\hat{L}^{(\text{B})}(\chi_{\text{B}})t}\overline{\mathbf{P}}_{\alpha\beta}'$$
$$\approx \left[1 - i\hat{L}_{\alpha\beta}^{(\text{int})}(\overline{\chi}_{\alpha\beta},\chi_{\text{B}})t - i\hat{L}^{(\text{B})}(\chi_{\text{B}})t\right]\overline{\mathbf{P}}_{\alpha\beta}'. \quad (A1)$$

Consequently, one gets

$$\int d\chi_{\text{B}} \, \rho_{\text{c}}(\chi_{\text{B}}|\chi)\left[1 - i\hat{L}_{\alpha\beta}^{(\text{int})}(\overline{\chi}_{\alpha\beta},\chi_{\text{B}})t - i\hat{L}^{(\text{B})}(\chi_{\text{B}})t\right]\overline{\mathbf{P}}_{\alpha\beta}'$$
$$= \overline{\mathbf{P}}_{\alpha\beta}' + \int d\chi_{\text{B}} \, \rho_{\text{c}}(\chi_{\text{B}}|\chi)\nabla_{\mathbf{q}}E_{\alpha\beta}^{(\text{int})}(\mathbf{Q},\mathbf{Q}_{\text{B}}) \, t, \quad (A2)$$

where the integral in the right-hand side of the equation can be approximated to $\mathbf{k}(\overline{\chi}_{\alpha\beta})t$. $\mathbf{k}(\overline{\chi}_{\alpha\beta})$ is in principle a dense matrix, but if there are no cross-correlation effects it becomes diagonal. Considering the case of no correlations between momenta and supposing that each momentum $\overline{p}_{\alpha\beta,i}'$ decays to zero for $t_i = \tau_{\text{dec},i}$, the following expression is obtained:

$$\mathbf{k}(\overline{\chi}_{\alpha\beta}) = \boldsymbol{\tau}_{\text{dec}}^{-1} \, \overline{\mathbf{p}}_{\alpha\beta}'. \quad (A3)$$

Finally, considering the inverse of the Taylor expansion, Eq. (16) is obtained,

$$\left(\mathbf{1} - \boldsymbol{\tau}_{\text{dec}}^{-1} \, t\right)\overline{\mathbf{p}}_{\alpha\beta}' = e^{-\boldsymbol{\tau}_{\text{dec}}^{-1} \, t} \, \overline{\mathbf{p}}_{\alpha\beta}'. \quad (A4)$$

APPENDIX B: APPROXIMATE CORRELATION FUNCTION OF THE MOMENTUM

In this appendix, an estimation of the τ_{dec} for a one-dimensional problem $\mathbf{X} = (q,p)$ is provided. In the hypothesis that

$$E_{\alpha\beta} \approx \frac{1}{2}k(q - q_{\text{eq}}), \quad (B1)$$

the probability density function associated with the mean PES is

$$\rho_{\text{eq}} = \frac{1}{Z} \, e^{-\frac{k}{2k_{\text{B}}T}(q-q_{\text{eq}})^2 - \frac{1}{2k_{\text{B}}Tg}p^2}. \quad (B2)$$

Changing the variables $\tilde{q} = \sqrt{\frac{k}{k_{\text{B}}T}}(q - q_{\text{eq}})$ and $\tilde{p} = \sqrt{\frac{1}{k_{\text{B}}Tg}}p$, the Fokker–Planck operator for the evolution on $E_{\alpha\beta}$ becomes

$$\hat{\Gamma} = -\begin{bmatrix}\frac{\partial}{\partial\tilde{q}} \\ \frac{\partial}{\partial\tilde{p}}\end{bmatrix}^{\text{tr}}\begin{bmatrix}0 & -\sqrt{\frac{k}{g}} \\ \sqrt{\frac{k}{g}} & \frac{\xi}{g}\end{bmatrix}\tilde{\rho}_{\text{eq}}\begin{bmatrix}\frac{\partial}{\partial\tilde{q}} \\ \frac{\partial}{\partial\tilde{p}}\end{bmatrix}\tilde{\rho}_{\text{eq}}^{-1} = \tilde{\nabla}_{\tilde{\mathbf{X}}}^{\text{tr}}\boldsymbol{\omega}\tilde{\rho}_{\text{eq}}\tilde{\nabla}_{\tilde{\mathbf{X}}}\tilde{\rho}_{\text{eq}}^{-1}, \quad (B3)$$

where $\tilde{\mathbf{X}} = (\tilde{q},\tilde{p})$ and $\tilde{\rho}_{\text{eq}} = (2\pi)^{-1}e^{-(\tilde{q}^2+\tilde{p}^2)/2}$. Considering the symmetrized Fokker–Planck operator,

$$\hat{\tilde{\Gamma}} = \tilde{\rho}_{\text{eq}}^{-1/2}\hat{\tilde{\Gamma}}\tilde{\rho}_{\text{eq}}^{1/2}, \quad (B4)$$

the following ladder operator is defined:

$$\hat{\mathbf{S}}^{\pm} = \begin{bmatrix}\hat{S}_{\tilde{q}}^{\pm} \\ \hat{S}_{\tilde{p}}^{\pm}\end{bmatrix} = \mp\begin{bmatrix}e^{\pm\tilde{q}^2/4}\,\frac{\partial}{\partial\tilde{q}}\,e^{\mp\tilde{q}^2/4} \\ e^{\pm\tilde{p}^2/4}\,\frac{\partial}{\partial\tilde{p}}\,e^{\mp\tilde{p}^2/4}\end{bmatrix}, \quad (B5)$$

so that $\hat{\tilde{\Gamma}} = \hat{\mathbf{S}}^+ \cdot \boldsymbol{\omega}\hat{\mathbf{S}}^-$. Then, the left and right eigenvalues of $\boldsymbol{\omega}$ are taken into account,

$$\boldsymbol{\omega}\mathbf{E} = \mathbf{E}\boldsymbol{\lambda}, \quad (B6)$$

$$\mathbf{F}^{\text{tr}}\boldsymbol{\omega} = \boldsymbol{\lambda}\mathbf{F}^{\text{tr}}, \quad (B7)$$

$$\mathbf{F}^{\text{tr}}\mathbf{E} = \mathbf{I}. \quad (B8)$$

In this way, the symmetrized Fokker–Planck operator is rewritten as

$$\hat{\tilde{\Gamma}} = \hat{\mathbf{O}}^+ \cdot \boldsymbol{\lambda} \hat{\mathbf{O}}^- = -\lambda_1 \hat{O}_1^+ \hat{O}_1^- - \lambda_2 \hat{O}_2^+ \hat{O}_2^-, \quad (B9)$$

where

$$\hat{\mathbf{O}}^+ = \mathbf{E}^{\text{tr}} \hat{\mathbf{S}}^+ \quad (B10)$$

$$\hat{\mathbf{O}}^- = \mathbf{F}^{\text{tr}} \hat{\mathbf{S}}^-. \quad (B11)$$

The eigenfunctions of $\hat{\tilde{\Gamma}}$ are

$$|n_1, n_2\rangle = (n_1! n_2!)^{-1/2} (\hat{O}_1^+)^{n_1} (\hat{O}_2^+)^{n_2} |0, 0\rangle, \quad (B12)$$

where $|0, 0\rangle = \tilde{\rho}_{\text{eq}}^{1/2}$ and the effect of the ladder operators is

$$(\hat{O}_1^+)^{m_1} |n_1, n_2\rangle = \sqrt{\frac{(n_1 + m_1)!}{n_1!}} |n_1 + m_1, n_2\rangle, \quad (B13)$$

$$(\hat{O}_1^-)^{m_1} |n_1, n_2\rangle = \sqrt{\frac{n_1!}{(n_1 - m_1)!}} |n_1 - m_1, n_2\rangle, \quad (B14)$$

provided that $m_1 \leq n_1$, otherwise the result is 0 (similar equations exist for operators acting on the second coordinate). Using these rules, one gets

$$\hat{\tilde{\Gamma}} |n_1, n_2\rangle = (\lambda_1 n_1 + \lambda_2 n_2 |n_1, n_2\rangle = \Lambda_{n_1, n_2} |n_1, n_2\rangle. \quad (B15)$$

The time-correlation function for the momenta becomes

$$C(t) = \frac{\langle \tilde{p} \tilde{\rho}_{\text{eq}}^{1/2} | e^{-\hat{\tilde{\Gamma}} t} | \tilde{p} \tilde{\rho}_{\text{eq}}^{1/2} \rangle}{\langle \tilde{p}^2 \tilde{\rho}_{\text{eq}} \rangle}$$

$$= \sum_{n_1, n_2} \sum_{n_1', n_2'} \langle \tilde{p} \tilde{\rho}_{\text{eq}}^{1/2} | n_1, n_2 \rangle$$

$$\times \langle \bar{n}_1, \bar{n}_2 | e^{-\hat{\tilde{\Gamma}} t} | n_1', n_2' \rangle \langle \bar{n}_1', \bar{n}_2' | \tilde{p} \tilde{\rho}_{\text{eq}}^{1/2} \rangle, \quad (B16)$$

where $|\bar{n}_1', \bar{n}_2'\rangle = (n_1! n_2!)^{-1/2} [(\hat{O}_1^-)^{n_1}]^{\dagger} [(\hat{O}_1^-)^{n_2}]^{\dagger} |0, 0\rangle$. Using the properties

$$\langle \bar{n}_1', \bar{n}_2' | n_1, n_2 \rangle, \quad (B17)$$

$$[\hat{O}_i^+, \hat{O}_j^+] = [\hat{O}_i^-, \hat{O}_j^-], \quad (B18)$$

$$[\hat{O}_i^+, \hat{O}_j^-] = \delta_{i,j}. \quad (B19)$$

Equation (B16) becomes

$$C(t) = \sum_{n_1, n_2} \langle \tilde{p} \tilde{\rho}_{\text{eq}}^{1/2} | n_1, n_2 \rangle \langle \bar{n}_1, \bar{n}_2 | \tilde{p} \tilde{\rho}_{\text{eq}}^{1/2} \rangle e^{-\Lambda_{n_1, n_2} t}. \quad (B20)$$

To compute the integrals in Eq. (B20), the expansion of $\tilde{p} \tilde{\rho}_{\text{eq}}^{1/2}$ is helpful

$$|\tilde{p} \tilde{\rho}_{\text{eq}}^{1/2}\rangle = \hat{S}_{\tilde{q}}^+ |0, 0\rangle = F_{1, \tilde{p}} \hat{O}_1^+ |0, 0\rangle + F_{2, \tilde{p}} \hat{O}_2^+ |0, 0\rangle$$

$$= F_{1, \tilde{p}} |1, 0\rangle + F_{2, \tilde{p}} |0, 1\rangle \quad (B21)$$

together with its conjugated complex given by

$$\langle \tilde{p} \tilde{\rho}_{\text{eq}}^{1/2} | = \langle \bar{1}, \bar{0} | E_{1, \tilde{p}} + \langle \bar{0}, \bar{1} | E_{2, \tilde{p}}. \quad (B22)$$

In this way, Eq. (B20) can be written as

$$C(t) = E_{1, \tilde{p}} F_{1, \tilde{p}} e^{-\Lambda_{1, 0} t} + E_{2, \tilde{p}} F_{2, \tilde{p}} e^{-\Lambda_{0, 1} t}. \quad (B23)$$

After computing the eigenvalues $\lambda_1 = \lambda_+$ and $\lambda_2 = \lambda_-$ of $\boldsymbol{\omega}$,

$$\lambda_\pm = \frac{\xi}{2g} \pm \frac{1}{2} \sqrt{\frac{\xi^2}{g^2} - 4\frac{k}{g}}, \quad (B24)$$

and imposing the condition $\mathbf{F}^{\text{tr}} \mathbf{E} = \mathbf{I}$, the left and right eigenvectors are obtained as

$$\mathbf{E}_1 = \frac{1}{\sqrt{\lambda_1^2 - k/g}} \begin{bmatrix} -\sqrt{k/g} \\ \lambda_1 \end{bmatrix} = \begin{bmatrix} E_{1, \tilde{q}} \\ E_{1, \tilde{p}} \end{bmatrix}, \quad (B25)$$

$$\mathbf{E}_2 = \frac{1}{\sqrt{\lambda_1^2 - k/g}} \begin{bmatrix} -\lambda_1 \\ \sqrt{k/g} \end{bmatrix} = \begin{bmatrix} E_{2, \tilde{q}} \\ E_{2, \tilde{p}} \end{bmatrix}, \quad (B26)$$

$$\mathbf{F}_1 = \frac{1}{\sqrt{\lambda_1^2 - k/g}} \begin{bmatrix} \sqrt{k/g} \\ \lambda_1 \end{bmatrix} = \begin{bmatrix} F_{1, \tilde{q}} \\ F_{1, \tilde{p}} \end{bmatrix}, \quad (B27)$$

$$\mathbf{F}_2 = -\frac{1}{\sqrt{\lambda_1^2 - k/g}} \begin{bmatrix} \lambda_1 \\ \sqrt{k/g} \end{bmatrix} = \begin{bmatrix} F_{2, \tilde{q}} \\ F_{2, \tilde{p}} \end{bmatrix}. \quad (B28)$$

Finally, the approximate time-correlation function is

$$C(t) = \frac{\lambda_1^2}{\lambda_1^2 - k/g} e^{-\lambda_1 t} - \frac{k/g}{\lambda_1^2 - k/g} e^{-\lambda_2 t}. \quad (B29)$$

REFERENCES

[1] J. Campeggio, R. Cortivo, and M. Zerbetto, "A multiscale approach to coupled nuclear and electronic dynamics. I. Quantum-stochastic Liouville equation in natural internal coordinates," J. Chem. Phys. **158**, 244104 (2023).

[2] A. Nassimi, S. Bonella, and R. Kapral, "Analysis of the quantum–classical Liouville equation in the mapping basis," J. Chem. Phys. **133**, 134115 (2010).

[3] R. Kapral, "Quantum–classical dynamics in a classical bath," J. Phys. Chem. A **105**, 2885 (2001).

[4] D. W. Howgate, "Calculation of nonradiative electron transition rates in a lattice-localized-electron system," Phys. Rev. **177**, 1358 (1969).

[5] J. Collins, "Non-radiative processes in crystals and in nanocrystals," ECS J. Solid State Sci. Technol. **5**, R3170 (2015).

[6] X. Zhou and B. J. Powell, "Quantitative calculations of the non-radiative rate of phosphorescent Ir(III) complexes," Phys. Chem. Chem. Phys. **22**, 27348 (2020).

[7] K. C. Mishra and J. Collins, "Formulation of radiative and nonradiative transitions of a polyatomic system within the crude adiabatic approximation," Opt. Mater.: X **15**, 100190 (2022).

[8] A. W. Kohn, Z. Lin, and T. Van Voorhis, "Toward prediction of nonradiative decay pathways in organic compounds I: The case of naphthalene quantum yields," J. Phys. Chem. C **123**, 15394 (2019).

[9] K. Shizu and H. Kaji, "Theoretical determination of rate constants from excited states: Application to benzophenone," J. Phys. Chem. A **125**, 9000 (2021).

[10] S. A. Egorov, E. Rabani, and B. J. Berne, "Nonradiative relaxation processes in condensed phases: Quantum versus classical baths," J. Chem. Phys. **110**, 5238 (1999).

[11] R. Grunwald and R. Kapral, "Decoherence and quantum–classical master equation dynamics," J. Chem. Phys. **126**, 114109 (2007).

[12] A. Polimeno, M. Zerbetto, and D. Abergel, "Stochastic modeling of macromolecules in solution. I. Relaxation processes," J. Chem. Phys. **150**, 184107 (2019).

[13] J. P. Rank and R. Kapral, "Decoherence and quantum–classical dynamics in a dissipative bath," J. Chem. Phys. **132**, 074106 (2010).

[14] S. J. Marrink, H. J. Risselada, S. Yefimov, D. P. Tieleman, and A. H. de Vries, "The MARTINI force field: Coarse grained model for biomolecular simulations," J. Phys. Chem. B **111**, 7812 (2007).

[15] S. J. Marrink and A. E. Mark, "Molecular dynamics simulation of the formation, structure, and dynamics of small phospholipid vesicles," J. Am. Chem. Soc. **125**, 15233 (2003).

[16] J. Campeggio, A. Polimeno, and M. Zerbetto, "DiTe2: Calculating the diffusion tensor for flexible molecules," J. Comput. Chem. **40**, 697 (2019).

[17] NAMD was developed by the Theoretical and Computational Biophysics Group in the Beckman Institute for Advanced Science and Technology at the University of Illinois at Urbana-Champaign.

[18] J. C. Phillips, D. J. Hardy, J. D. C. Maia, J. E. Stone, J. V. Ribeiro, R. C. Bernardi, R. Buch, G. Fiorin, J. Hénin, W. Jiang, R. McGreevy, M. C. R. Melo, B. K. Radak, R. D. Skeel, A. Singharoy, Y. Wang, B. Roux, A. Aksimentiev, Z. Luthey-Schulten, L. V. Kalé, K. Schulten, C. Chipot, and E. Tajkhorshid, "Scalable molecular dynamics on CPU and GPU architectures with NAMD," J. Chem. Phys. **153**, 044130 (2020).

[19] G. Fiorin, M. L. Klein, and J. Hénin, "Using collective variables to drive molecular dynamics simulations," Mol. Phys. **111**, 3345 (2013).

[20] J. C. Tully, "Molecular dynamics with electronic transitions," J. Chem. Phys. **93**, 1061 (1990).

[21] E. J. Kansa, "Multiquadrics—A scattered data approximation scheme with applications to computational fluid-dynamics—I surface approximations and partial derivative estimates," Comput. Math. Appl. **19**, 127–145 (1990).

[22] E. J. Kansa, "Multiquadrics—A scattered data approximation scheme with applications to computational fluid-dynamics—II solutions to parabolic, hyperbolic and elliptic partial-differential equations," Comput. Math. Appl. **19**, 147 (1990).

[23] B. Sarler and R. Vertnik, "Meshfree explicit local radial basis function collocation method for diffusion problems," Comput. Math. Appl. **51**, 1269 (2006).